Phys. Med. Biol. **55** (2010) N383–N394 doi:10.1088/0031-9155/55/13/N02

NOTE

A fast time-domain algorithm for the assessment of tissue blood flow in laser-Doppler flowmetry

Tiziano Binzoni[1,2], **Chandra Sekhar Seelamantula**[3] **and Dimitri Van De Ville**[2,4]

[1] Département des Neurosciences Fondamentales, University of Geneva, Switzerland
[2] Département de l'Imagerie et des Sciences de l'Information Médicale, University Hospital, Geneva, Switzerland
[3] Department of Electrical Engineering, Indian Institute of Science, Bangalore, India
[4] Institute of Bioengineering, Ecole Polytechnique Fédérale de Lausanne (EPFL), Switzerland

E-mail: tiziano.binzoni@unige.ch

Received 18 February 2010, in final form 18 May 2010
Published 9 June 2010
Online at stacks.iop.org/PMB/55/N383

Abstract

In this study, we derive a fast, novel time-domain algorithm to compute the *n*th-order moment of the power spectral density of the photoelectric current as measured in laser-Doppler flowmetry (LDF). It is well established that in the LDF literature these moments are closely related to fundamental physiological parameters, i.e. concentration of moving erythrocytes and blood flow. In particular, we take advantage of the link between moments in the Fourier domain and fractional derivatives in the temporal domain. Using Parseval's theorem, we establish an exact analytical equivalence between the time-domain expression and the conventional frequency-domain counterpart. Moreover, we demonstrate the appropriateness of estimating the zeroth-, first- and second-order moments using Monte Carlo simulations. Finally, we briefly discuss the feasibility of implementing the proposed algorithm in hardware.

(Some figures in this article are in colour only in the electronic version)

1. Introduction

Assessing the number of moving erythrocytes and blood flow (or perfusion) using laser-Doppler flowmetry (LDF) relies on the use of the zeroth- ($\langle\omega^0\rangle$) and the first-order ($\langle\omega^1\rangle$) moments of the power spectrum of the photoelectric current $i(t)$ (for a review cf Briers (2001) and Humeau *et al* (2007)).

While the original LDF theory was developed for a simple point-source point-detector configuration, it has been shown experimentally and theoretically that it can also be applied—with acceptable accuracy—to more sophisticated geometries such as for full-field laser-Doppler imagers (Serov *et al* 2002, 2005, Briers 2007, Binzoni and Van De Ville 2008,

Draijer *et al* 2009a, Raabe *et al* 2009). To obtain images related to blood perfusion in real time, this new LDF hardware requires the nearly-simultaneous computation of thousands of power spectra using Fourier transform (FT) algorithms and their respective moments (e.g. a 512 × 512 image would require 262 144 such computations). In this context, the main bottleneck of the classical moment calculation algorithm is the utilization of the FT. Even with dedicated hardware to calculate the FT, the task remains difficult and expensive. For this reason, Draijer *et al* (2009b) have introduced a time-domain algorithm, which does not require the FT, allowing the estimation of $\langle\omega^1\rangle$ and thus the blood flow. This algorithm is derived by making an 'intuitive' approximation of the actual moments as computed using the FT. This limitation makes it difficult to take advantage of the large theoretical and experimental knowledge accumulated during years on the physiological significance of the different moments of order n ($\langle\omega^n\rangle$), which are all linked to the concentration of moving erythrocytes and blood flow.

Our aim in this note is to derive an exact analytical expression for the moments in the time domain, and to use the related numerical algorithm for computing $\langle\omega^n\rangle$, $n \in \{0, 1, 2, \ldots\}$. Here, we exploit previous theoretical findings (Bonner and Nossal 1981, Binzoni *et al* 2004), which have shown that $\langle\omega^0\rangle$ and $\langle\omega^2\rangle$ allow us to assess the number and flow of red blood cells. This particular point has been proven on a set of synthetic $i(t)$ generated by Monte Carlo simulations (Binzoni *et al* 2009) that were derived from a large range of physiological values. The potential limitations on the maximum speed of the LDF-based instrumentation and the possible implementation of the proposed algorithm directly in hardware is also discussed. The present work represents a step further towards new time-domain algorithms for LDF that are computationally more efficient than straightforward fast Fourier approaches.

2. Material and methods

2.1. Analytical equation for $\langle\omega^n\rangle$ in the time domain

The nth-order moment of the power spectrum of $i(t)$ is conventionally defined in LDF as

$$\langle\omega^n\rangle := 2\int_0^\infty \omega^n \left|\int_{-\infty}^{\infty} [i(t) - i_o]\, \mathrm{e}^{-\mathrm{i}\omega t}\, \mathrm{d}t\right|^2 \mathrm{d}\omega, \tag{1}$$

where i_o is the dc component of the photo-electric current defined as

$$i_o = \lim_{T\to+\infty} \frac{1}{2T}\int_{-T}^{T} i(t)\, \mathrm{d}t, \tag{2}$$

and the Roman i is the imaginary number. From the numerical point of view, the computationally expensive part in equation (1) is the FT. Here, we eliminate the FT by first rewriting (1) as

$$\langle\omega^{2p}\rangle = 2\int_0^\infty \left|(\mathrm{i}\omega)^p \int_{-\infty}^{\infty} [i(t) - i_o]\, \mathrm{e}^{-\mathrm{i}\omega t}\, \mathrm{d}t\right|^2 \mathrm{d}\omega, \tag{3}$$

where $n = 2p$. We identify the fractional derivative of order $p \in \{0, 1/2, 1, 3/2, \ldots\}$ in the Fourier domain and consequently, equation (1) can be transformed into

$$\langle\omega^{2p}\rangle = 2\int_0^\infty \left|\int_{-\infty}^{\infty} \frac{\mathrm{d}^p}{\mathrm{d}t^p}\, [i(t) - i_o]\, \mathrm{e}^{-\mathrm{i}\omega t}\, \mathrm{d}t\right|^2 \mathrm{d}\omega, \tag{4}$$

and thanks to the Parseval's relation, we have that

$$\langle\omega^{2p}\rangle = 2\int_0^\infty \left|\frac{\mathrm{d}^p}{\mathrm{d}t^p}\, [i(t) - i_o]\right|^2 \mathrm{d}t. \tag{5}$$

Mathematically, the fractional derivative is a convolution operator that is defined in the sense of distributions in the Fourier domain (Podlubny 1999).

Numerical calculation of the integral in equation (5) is in principle faster than its counterpart in equation (1) because we got rid of the inner integral that corresponds to the FT. While classical derivatives, $p \in \{0, 1, \ldots\}$, can be computed efficiently in the time domain, there is a difficulty in making such an association in the context of fractional derivatives for $p \in \{1/2, 3/2, 5/2, \ldots\}$, which are relatively time consuming to compute, even with approximated fast algorithms (Galucio *et al* 2006). For this reason, we investigate in detail in the next section how the moments associated with classical derivatives can be used to retrieve physiological information.

2.2. *Link between* $\langle\omega^n\rangle$ *and the physiological parameters*

In their scholarly paper, Bonner and Nossal (1981) have established a relationship between $\langle\omega^n\rangle$, the tissue root mean square velocity $\langle V_{\text{Brown}}^2\rangle^{1/2}$ of the erythrocytes and the average number of collisions a detected photon makes with moving cells ($\bar{m}$). Recently, this model has been generalized to include the presence of a supplementary bulk movement of the erythrocytes by introducing a translational velocity term ($\vec{V}_{\text{trans}}$) in the description of $\langle\omega^n\rangle$ (Binzoni *et al* 2004). For the purpose of our analysis, we state here the first three equations correlating the physiological parameters with $\langle\omega^0\rangle$, $\langle\omega^1\rangle$ and $\langle\omega^2\rangle$ (see the appendix and equations (27)–(29) from Binzoni *et al* 2004):

$$\langle\omega^0\rangle = c_1(1 - \mathrm{e}^{-2\bar{m}}), \tag{6}$$

$$\langle\omega^1\rangle = \frac{c_1}{c_2}\left[\left(\frac{1}{3}\frac{\sqrt{3}}{\langle V_{\text{Brown}}^2\rangle^{-\frac{1}{2}}} + \frac{1}{8}\frac{\sqrt{3}\|\vec{V}_{\text{trans}}\|^2}{\langle V_{\text{Brown}}^2\rangle^{\frac{1}{2}}} + o(\|\vec{V}_{\text{trans}}\|^4)\right)\bar{m} + \left(\frac{1}{6}\frac{\sqrt{3}}{\langle V_{\text{Brown}}^2\rangle^{-\frac{1}{2}}} - \frac{1}{16}\frac{\sqrt{3}\|\vec{V}_{\text{trans}}\|^2}{\langle V_{\text{Brown}}^2\rangle^{\frac{1}{2}}} + o(\|\vec{V}_{\text{trans}}\|^4)\right)\bar{m}^2\right] + o(\bar{m}^3), \tag{7}$$

$$\langle\omega^2\rangle = \frac{c_1}{(c_2)^2}\left(\frac{1}{3}\langle V_{\text{Brown}}^2\rangle + \frac{1}{4}\|\vec{V}_{\text{trans}}\|^2\right)\bar{m}, \tag{8}$$

where c_1 and c_2 are constants (their significance is not crucial to our analysis here) and $o(\cdot)$ represents the remaining terms for the variable appearing in the parenthesis. It must be noted that equations (6) and (8) are exact expressions whereas equation (7) is an infinite series expansion in $\|\vec{V}_{\text{trans}}\|$ and $\bar{m}$. If $\|\vec{V}_{\text{trans}}\| = 0$, then equations (6)–(8) reduce to the original Bonner and Nossal (1981) model for $\langle\omega^n\rangle$, $n \in \{0, 1, 2\}$, as it should. It is clear that equations (6) and (8) have two major advantages: (1) they are simple and exact and; (2) they establish a correspondence with equation (5) for the case where the order of the derivative is a positive integer, thus eliminating the problem associated to the numerical implementation of fractional derivatives.

The utilization of equations (6) and (8) appears to be the best strategy from the numerical point of view. For this reason, by exploiting a known theoretical framework (Bonner and Nossal 1981, Binzoni *et al* 2004) we investigate next if $\langle\omega^0\rangle$ and $\langle\omega^2\rangle$ can potentially yield information about the number of moving erythrocytes and blood flow, the latter parameter being classically extracted from $\langle\omega^1\rangle$. By Taylor-series expansion of the right-hand side of equation (6) we get

$$\langle\omega^0\rangle = c_1\left(2\bar{m} - 2\bar{m}^2 + \tfrac{4}{3}\bar{m}^3 + o(\bar{m}^4)\right), \tag{9}$$

and by considering only the first order for $\bar{m}$ ($\bar{m}$ is classically considered to be small), $\langle\omega^0\rangle$ is approximated by $\langle\omega^0\rangle_{o(\bar{m}^2)}$ and turns out to be proportional to

$$\langle\omega^0\rangle \approx \langle\omega^0\rangle_{o(\bar{m}^2)} \propto \bar{m}. \tag{10}$$

This is a well-known result where $\bar{m}$ represents the average number of collisions that a detected photon makes with moving cells. According to the classical theory, $\bar{m}$ is also proportional to the concentration or number of the moving erythrocytes present in the measured region of interest (see e.g. Binzoni *et al* (2006)). In practice, laser-Doppler instruments can monitor the 'concentration' (in arbitrary units) of moving red blood cells since $\bar{m}$ can be obtained from equation (5) for $p = 0$. Thus, equation (10) shows that there is a link between $\langle\omega^0\rangle$ and the number of moving erythrocytes, but we still need to calculate the blood flow. The blood flow can be assessed by observing that

$$\langle\omega^0\rangle\sqrt{\frac{\langle\omega^2\rangle}{\langle\omega^0\rangle}} \approx \langle\omega^0\rangle_{o(\bar{m}^2)}\sqrt{\frac{\langle\omega^2\rangle}{\langle\omega^0\rangle_{o(\bar{m}^2)}}} \propto \bar{m}\sqrt{\frac{1}{3}\left\langle V_{\text{Brown}}^2\right\rangle + \frac{1}{4}\|\vec{V}_{\text{trans}}\|^2}, \tag{11}$$

where $\langle\omega^0\rangle$ and $\langle\omega^2\rangle$ have been expressed using equations (10) and (8), respectively. Equation (11) expresses blood flow because we have a general speed term ($\sqrt{.}$) times a 'blood volume' ($\bar{m}$). It remains to be tested whether $\sqrt{.}$ reflects the actual mean speed of the erythrocytes $\langle\|\vec{V}\|\rangle$ in the investigated tissue. In fact, $\langle\|\vec{V}\|\rangle$ for a given set of parameters $\left\langle V_{\text{Brown}}^2\right\rangle^{1/2}$ and $\vec{V}_{\text{trans}}$ (normal velocity distribution plus a bulk translational movement) can be written as (equation (14) in Binzoni and Van De Ville 2008)

$$\langle\|\vec{V}\|\rangle = \frac{\sqrt{6}}{3}\frac{\left\langle V_{\text{Brown}}^2\right\rangle^{1/2}}{\sqrt{\pi}}\,\mathrm{e}^{-\frac{3}{2}\frac{\|\vec{V}_{\text{trans}}\|^2}{\langle V_{\text{Brown}}^2\rangle}}\left(\|\vec{V}_{\text{trans}}\| + \frac{\left\langle V_{\text{Brown}}^2\right\rangle^{1/2}}{3\|\vec{V}_{\text{trans}}\|}\right)\operatorname{erf}\left(\frac{\sqrt{6}}{2}\frac{\|\vec{V}_{\text{trans}}\|}{\left\langle V_{\text{Brown}}^2\right\rangle^{1/2}}\right), \tag{12}$$

for $\|\vec{V}_{\text{trans}}\| \neq 0$ and

$$\lim_{\|\vec{V}_{\text{trans}}\|\to 0}\langle\|\vec{V}\|\rangle = \frac{2\sqrt{6}}{3}\frac{\left\langle V_{\text{Brown}}^2\right\rangle^{1/2}}{\sqrt{\pi}}. \tag{13}$$

Equation (13) reproduces exactly the mean velocity of the Bonner and Nossal (1981) model, where $\|\vec{V}_{\text{trans}}\|$ is considered to be zero. When $\|\vec{V}_{\text{trans}}\| = 0$, the $\sqrt{.}$ factor of equation (11) (up to a proportionality constant $\sqrt{8/\pi}$) is equal to the actual $\langle\|\vec{V}\|\rangle$ (equation (13)). When $\|\vec{V}_{\text{trans}}\| \neq 0$, an analytical comparison giving a good intuition of the problem is more difficult to perform. For this reason, a numerical comparison between $\sqrt{.}$ (equation (11)) and $\langle\|\vec{V}\|\rangle$ (equation (12)) is reported in figure 1.

Even in this case, we obtain a reasonable linear relationship between speeds (with the proportionality factor $\sqrt{8/\pi}$) and in particular, as expected, when $\|\vec{V}_{\text{trans}}\|$ is small. Figure 1 suggests that equation (11) is a good estimator for the blood flow (if $\|\vec{V}_{\text{trans}}\| = 0$, then the estimation is exact, by definition).

In conclusion, the analysis of sections 2.1 and 2.2 together with the classical theoretical interpretation of LDF encourages us to use $\langle\omega^0\rangle$ and $\langle\omega^2\rangle$ to estimate the number of moving erythrocytes and blood flow. We will further validate this hypothesis in the following sections by considering Monte Carlo simulations.

2.3. Monte Carlo simulation of $i(t)$

To further corroborate whether $\langle\omega^0\rangle$ and $\langle\omega^2\rangle$ reflect the desired physiological parameters, we compute them for a set of simulated photo-currents $i(t)$ (i.e. the signal as produced by a real LDF instrument) derived from known $\bar{m}$, $\left\langle V_{\text{Brown}}^2\right\rangle$ and $\|\vec{V}_{\text{trans}}\|$ values. Considering that this

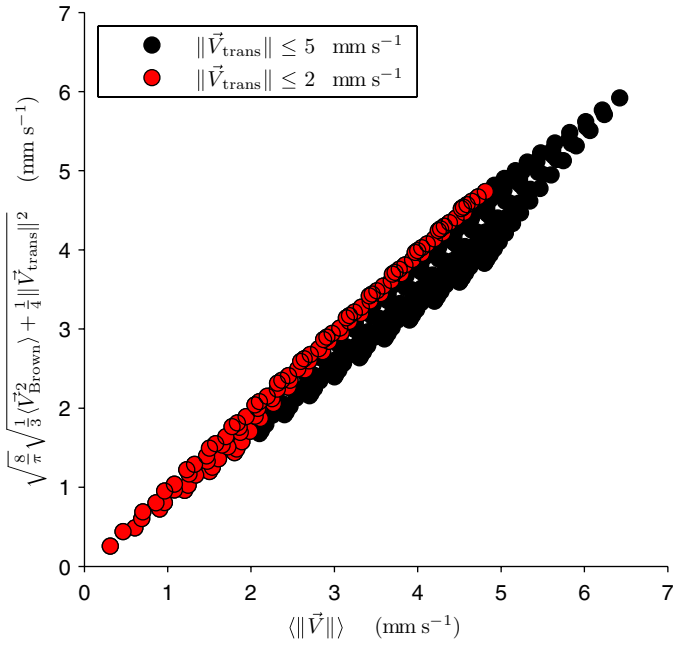

Figure 1. Comparison of the exact mean velocity ($\langle\|\vec{V}\|\rangle$, equation (12)) for the erythrocytes (Brownian motion (normal distribution), $\left\langle V^2_{\rm Brown}\right\rangle^{1/2}$, plus a bulk translational velocity, $\vec{V}_{\rm trans}$) and the velocity estimated with the $\sqrt{\cdot}$ term appearing in equation (11). The proportionality factor $\sqrt{8/\pi}$ allows us to compare the data in mm s^{-1}. Each point represents a particular combination of physiological parameters.

condition is impossible to fulfill in an experimental scenario, we have generated a large set of different $i(t)$ by Monte Carlo simulation (Binzoni *et al* 2009).

In summary, a virtual tissue phantom was represented by a semi-infinite medium. The LDF was a simple point-source/detector configuration, with the source normal to the plane and an annular detector of 75 μm width. The interoptode spacing (0.5 mm) was defined as the distance between the point-source and the middle point of the annular detector. The number of photon packets generated for obtaining one $i(t)$ (one simulation) was $N_{\rm packet} = 18 \times 10^6$. Following equation (13) in Binzoni *et al* (2009), we can express $i(t)$ as

$$i(t) \propto \left| \sum_{n=1}^{N_{\rm packet}} [\sqrt{W(\Delta\omega_n)}\, {\rm e}^{{\rm i}\Phi(\omega_0+\Delta\omega_n)}]\, {\rm e}^{-{\rm i}\Delta\omega_n t} \right|^2, \tag{14}$$

where $\Delta\omega_n$ are the accumulated Doppler shifts, $W(\cdot)$ the weights of the photon packets reaching the detector and $\Phi(\omega_0 + \Delta\omega_n) \in [0, 2\pi]$ the phase factors that are uniformly independently distributed random variables satisfying the constraint

$$\omega_1 = \omega_2 \quad \Longrightarrow \quad \Phi(\omega_1) = \Phi(\omega_2). \tag{15}$$

From each simulation, 100 different $i(t)$ realizations taking into account the possible random phase accumulated by the photons along their travel inside the tissue were obtained (Binzoni *et al* 2009). Intuitively, the random phase manifests itself as the noise-like appearance of $i(t)$ and explains also why it is experimentally necessary to average many power spectra

(obtained from different $i(t)$) to obtain one noise-free spectrum (in the present case we have the choice to average from 1 up to 100 spectra); the chosen number of averages is denoted by N_{avg}. The absorption coefficient (μ_{a}), the reduced scattering coefficient (μ_{s}'), the refractive index (n), the anisotropy parameter (g) and the wavelength (λ) were set to 0.025 mm^{-1}, 0.5 mm^{-1}, 1.4, 0.9 and 800 nm, respectively, for all the simulations. The refractive index for the air was taken to be unity. The remaining parameters were $P_{\text{move}} \in \{0.025, 0.05, 0.075, 0.1, 0.125, 0.15\}$, $\left\langle V_{\text{Brown}}^2 \right\rangle^{1/2} \in \{1, 2, 3, 4\}$ mm s^{-1} and $\|\vec{V}_{\text{trans}}\| \in \{0, 1, 2, 3, 4\}$ mm s^{-1}, where P_{move} is related to the fraction of scatterers (erythrocytes) moving inside the tissue and can be seen as the probability for a photon packet to interact with a moving particle. For a fixed interoptode distance we have (Binzoni and Van De Ville 2008)

$$P_{\text{move}} \propto \bar{m}, \tag{16}$$

and for this reason P_{move} will be chosen to interpret the results. The chosen set of parameters is representative for a skeletal muscle tissue (Ferreira *et al* 2007).

The sampling frequency for $i(t)$ was $\nu_{\text{s}} = 40$ kHz with the number of sampling points being N_{s} (see section 3).

2.4. Numerical computation of $\langle\omega^0\rangle$ and $\langle\omega^2\rangle$

The numerical algorithm for $\langle\omega^0\rangle$ and $\langle\omega^2\rangle$ can be easily implemented by rewriting equation (5) for $p = 0$ as (see the appendix)

$$\langle\omega^0\rangle \propto \sum_{n=0}^{N_{\text{s}}-1} (i(nt_{\text{s}}) - i_o)^2, \tag{17}$$

where $t_{\text{s}} = 1/\nu_{\text{s}}$ is the sampling time and

$$i_o = \frac{1}{N_{\text{s}}} \sum_{n=0}^{N_{\text{s}}-1} i(nt_{\text{s}}). \tag{18}$$

Equation (5) for $p = 1$ becomes

$$\langle\omega^2\rangle \propto \sum_{n=0}^{N_{\text{s}}-2} [i((n+1)t_{\text{s}}) - i(nt_{\text{s}})]^2, \tag{19}$$

where the first-order derivative has been approximated by using the first-order finite difference. Since experimentally LDF cannot lead to absolute values, the proportionality constants are neglected. It must be noted that equations (17) and (19) essentially give the same solution, for $n = 0$ and $n = 2$, as the classical direct numerical implementation of equation (1) using the FT, up to the discretization of the derivative, whose effect can be neglected at the chosen sampling rate. There is no doubt that the implementation related to equations (17) and (19) are simpler and faster than the FT-based algorithm.

When using a real LDF instrument, there is the inevitable acquisition noise and noise-like influence of the random phase on $i(t)$ (Binzoni *et al* 2009). It therefore becomes necessary to average many $\langle\omega^n\rangle$ to obtain a reliable value. We denote the average $\langle\omega^n\rangle$ value, for N_{avg} different samples, as $\overline{\langle\omega^n\rangle}$.

3. Results

As we have shown mathematically, expressions (1) and (5) are identical and both lead to $\langle\omega^n\rangle$ ($n \in \{1, 2, 3, \ldots\}$). As mentioned in section 2.4, the only difference between the FT-based

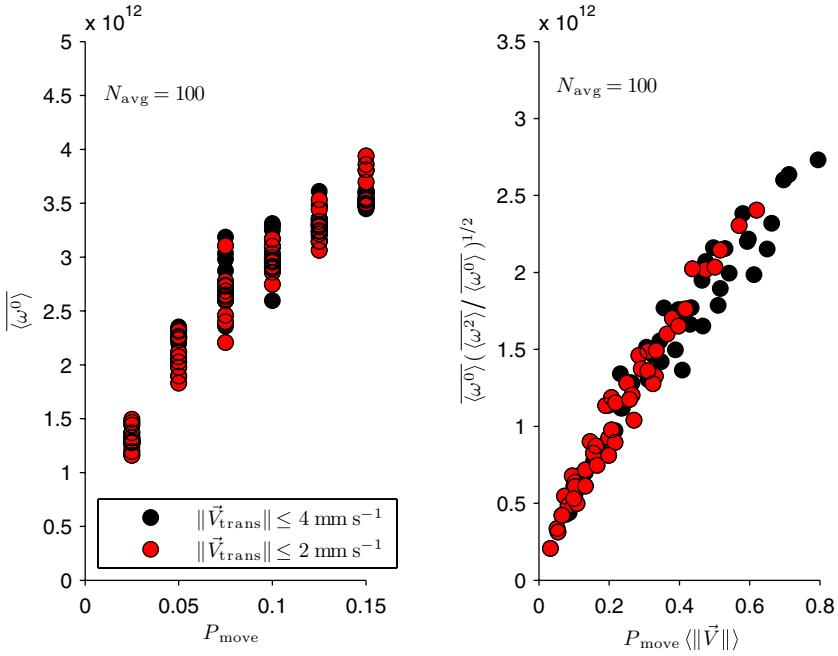

Figure 2. The number of $i(t)$ samples used to build each dot on the figure was $N_s = 1024$. The parameters $\overline{\langle\omega^0\rangle}$ and $\overline{\langle\omega^2\rangle}$ represent the average zero- and second-order moments computed using the fast algorithm represented by equations (17) and (19). For the average, N_{avg} different $\langle\omega^0\rangle$ or $\langle\omega^2\rangle$ were utilized. This tests the underlying hypothesis of equation (10). Left panel: relationship between the theoretically known number of moving red blood cells (proportional to P_{move} and classically representing the 'blood volume') and the same value estimated by the average zero moment, $\overline{\langle\omega^0\rangle}$. Right panel: relationship between the theoretically known 'blood flow' (proportional to $P_{move}\langle\|\vec{V}\|\rangle$) and the same values estimated using the expression $\overline{\langle\omega^0\rangle}(\overline{\langle\omega^2\rangle}/\overline{\langle\omega^0\rangle})^{1/2}$. This tests the underlying hypothesis of equation (11).

algorithm and the proposed time-domain approach is the finite-difference approximation of the derivative operator. Using our simulation data, we found a complete equivalence up to numerical accuracy.

As shown in figure 2, $\overline{\langle\omega^0\rangle}$ and $\overline{\langle\omega^2\rangle}$ computed using equations (17) and (19) are proper estimates of the number of moving erythrocytes (proportional to P_{move}) and blood flow (proportional to $P_{move}\langle\|\vec{V}\|\rangle$), respectively. Moreover, as postulated in section 2, the quantity $\overline{\langle\omega^0\rangle}(\overline{\langle\omega^2\rangle}/\overline{\langle\omega^0\rangle})^{1/2}$ appears to effectively estimate the blood flow ($P_{move}\langle\|\vec{V}\|\rangle$). Figure 2 (left panel) correctly reproduces the expected behaviour where the data appear to be slightly exponential (equation (6)), thus linear for small $\bar{m}$ (equation (10)), and where P_{move} and $\bar{m}$ are related through equation (16). These results have been obtained with a relatively small number of samples of $i(t)$ ($N_s = 1024$). An average of $N_{avg} = 100$ measurements was found to be necessary. In practice, this corresponds to an acquisition time for a given point in figure 2 of $N_s\nu_s^{-1}N_{avg} = 2.56$ s (data processing not included).

Figure 3 shows the same data as in figure 2 but for the parameter $N_{avg} = 10$. In this case the acquisition time reduces to 0.256 s and, as expected, the data are more scattered. From a practical point of view, the estimation of the number of moving erythrocytes P_{move} seems to be slightly more affected by the phase noise (for small N_{avg}) than the blood flow $P_{move}\langle\|\vec{V}\|\rangle$.

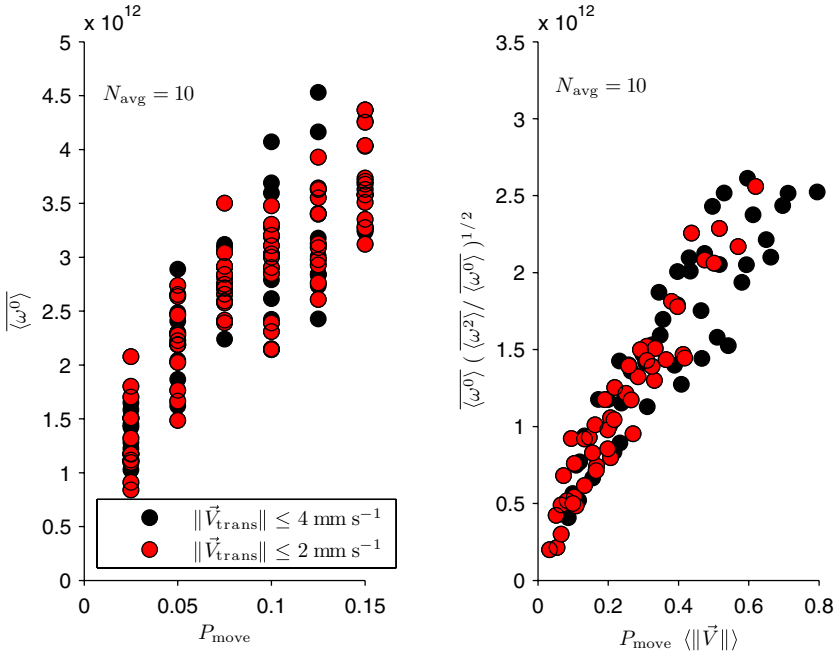

Figure 3. Same as in figure 2 but $N_{avg} = 10$.

4. Discussion and conclusions

In the present work, we have shown that it is possible to deduce (in relative units) the number of moving erythrocytes and the blood flow from $\overline{\langle\omega^0\rangle}$ and $\overline{\langle\omega^2\rangle}$. For this purpose, a new and fast time-domain algorithm has been derived, starting from the exact expression of $\overline{\langle\omega^0\rangle}$ and $\overline{\langle\omega^2\rangle}$. The analytical model developed by Bonner and Nossal (1981) and Binzoni *et al* (2004) has been utilized as a path that has brought us to the expression $\overline{\langle\omega^0\rangle}(\overline{\langle\omega^2\rangle}/\overline{\langle\omega^0\rangle})^{1/2}$ for the blood flow.

4.1. The maximum speed limit of a real-time LDF

As reported in section 3, the 'noise-like' component of $i(t)$ is an intrinsic property of LDF measurements and requires us to average N_{avg} moments to obtain a reliable result. As already explained elsewhere (Binzoni *et al* 2009), the presence of this 'noise-like' component is due to the random phase accumulated by the photons before reaching the detector. This is a pure physical phenomenon generated by the interaction between the biological tissue and the photons. Thus, even for an ideal LDF instrument, with noise-free hardware, we still need to average out this component. This means that the acquisition time increases and that the computing time must be added to this value. For this reason, it is necessary to experimentally find the best compromise for the choice of N_s, N_{avg} and ν_s (frame rate in the case of an imager). Thus, for real-time systems, the value $N_s \nu_s^{-1} N_{avg}$ represents a theoretical lower bound on the speed of the instrument.

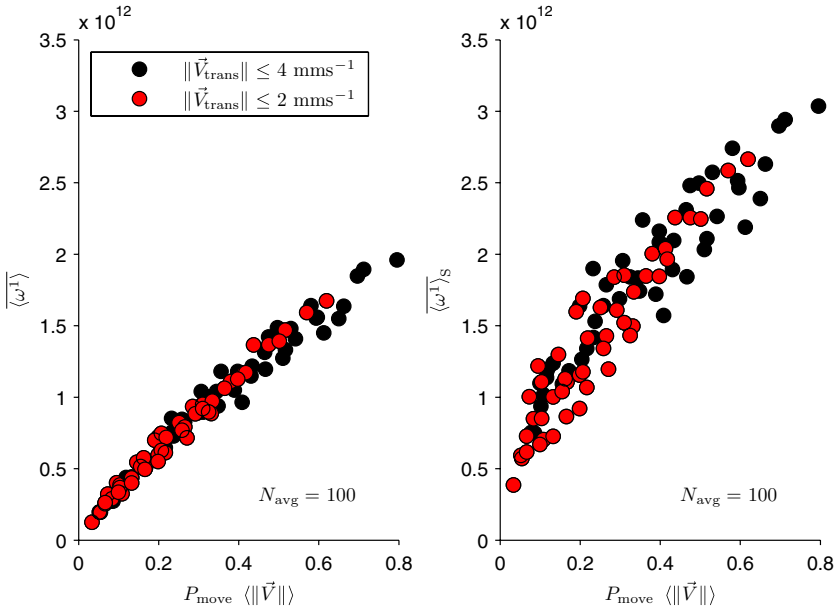

Figure 4. Same parameters as in figure 2. Left panel: average first-order moment ($\overline{\langle\omega^1\rangle}$) computed using equation (21) as a function of the blood flow ($P_{\rm move}\langle\|\vec{V}\|\rangle$). Right panel: average first-order moment ($\overline{\langle\omega^1\rangle}_{\rm S}$) computed using equation (22) as a function of the blood flow.

4.2. Outlook on time-domain algorithms

For the sake of completeness we present here the derivation of $\langle\omega^1\rangle$ obtained using the time-domain equation (5) with $p = 1/2$. This algorithm is obviously not fast; however, it is an exact algorithm reproducing $\langle\omega^1\rangle$ as obtained directly by the FT. This allows us to explicitly show the quality of the estimation of the blood flow using $\langle\omega^1\rangle$ (i.e. the classical approach) and compare it with its time-domain counterpart. To this end, equation (5) becomes

$$\langle\omega^1\rangle = 2\int_0^\infty \left|\frac{\mathrm{d}^{1/2}}{\mathrm{d}t^{1/2}}\left[i(t) - i_o\right]\right|^2 \mathrm{d}t. \tag{20}$$

By using the Grünwald–Letnikov approach to the fractional derivative (Podlubny 1999), equation (20) can be discretized as

$$\langle\omega^1\rangle \propto \sum_{n=0}^{N_s-1}\left[\sum_{j=o}^{n}(-1)^j \frac{\Gamma(3/2)}{\Gamma(j+1)\Gamma(3/2-j)}\{i([n-j]\,t_s) - i_o\}\right]^2 \tag{21}$$

where Γ is the Gamma function. It must be noted that the Grünwald–Letnikov algorithm (suitably combined with equation (5)) gives the solution found in equations (17) and (19) for $p = 0$ and $p = 1$, respectively, and thus is in accordance with the present approach. Other numerical approaches to evaluating the fractional derivatives can also be used, but this subject is beyond the scope of this note.

In figure 4, the average $\langle\omega^1\rangle$ (equation (21)) is shown as a function of the blood flow ($P_{\rm move}\langle\|\vec{V}\|\rangle$). It appears, in agreement with the classical theory, that $\overline{\langle\omega^1\rangle}$ is a good estimator but this result shows that $\overline{\langle\omega^2\rangle}$ is also an equally good estimator. It is possible that the introduction of a fast method for the fractional derivative of order $p = 1/2$ would render $\overline{\langle\omega^1\rangle}$

more interesting; however, this is a matter of further investigation. It is instructive at this point to consider the first algorithm historically introduced for the estimation of $\overline{\langle\omega^1\rangle}$ in the time domain for LDF (equation (11) in Draijer *et al* (2009b)) as follows:

$$\langle\omega^1\rangle_S \propto \sum_{n=0}^{N_s-1} |i(nt_s)\{i([n+1]t_s) - i(nt_s)\}| . \tag{22}$$

This equation has never been validated on Monte Carlo data and thus we reproduce the results in figure 4. In practice, we can observe that equation (22) coherently reproduces the behaviour of the blood flow but it appears to be less accurate. This is an expected finding since equation (22) was derived 'intuitively' as a reasonably good approximation of $\overline{\langle\omega^1\rangle}$.

4.3. Feasibility of hardware implementation

As mentioned in the introduction, despite the fact that the classical FT approach was developed for a simple point-source point-detector configuration, it has been applied as the core algorithm for full-field laser-Doppler imagers (Serov *et al* 2002, 2005, Briers 2007, Binzoni and Van De Ville 2008, Draijer *et al* 2009a, Raabe *et al* 2009). We have shown that the proposed novel time-domain algorithm (equation (5)) for computing the moments $\langle\omega^0\rangle$ and $\langle\omega^2\rangle$ is equivalent to the FT approach (equation (1)). The numerical implementation of equations (17) (i.e. estimation of the concentration of erythrocytes) and (19) (i.e. estimation of the 'blood flow') only requires basic arithmetic operations, which can be realized using elementary adders, subtractors, squarers/multipliers and accumulators. The algorithms can be programmed using Verilog/VHDL (Ciletti 2009, Roth and John 2007) and can be subsequently synthesized, placed and routed for field-programmable gate arrays (FPGAs)/application-specific integrated circuits (ASICs). Using these basic blocks on a pixel-by-pixel basis enables massive parallelization, which can potentially generate perfusion images in real time (Morgan *et al* 2010).

Acknowledgments

The authors would like to thank the 'Faculté de Médecine' of Geneva for the Mimosa grant that enabled the computer cluster to be set up. This work was supported in part (DVDV) by the Swiss National Science Foundation (grant PP00P2-123438).

Appendix

A.1. The Grünwald–Letnikov fractional derivative

The fractional derivative of order p of the photo-electric current $i(t)$, sampled at the time points $t = jt_s$, where $j = \{1, 2, \ldots, N_s\}$, can be written using the Grünwald–Letnikov scheme as (equation (2.10) in Podlubny (1999))

$$\frac{\mathrm{d}^p}{\mathrm{d}t^p} i(nt_s) := \frac{1}{t_s^p} \sum_{j=0}^{n} (-1)^j \begin{bmatrix} p \\ j \end{bmatrix} i([n-j]t_s), \tag{A.1}$$

where

$$\begin{bmatrix} p \\ j \end{bmatrix} := \frac{\Gamma(p+1)}{\Gamma(j+1)\Gamma(p+1-j)}. \tag{A.2}$$

In this manner, by using equations (A.1) and (A.2), one obtains the derivatives for p equal to 0, 1/2 and 1:

$$\frac{\mathrm{d}^0}{\mathrm{d}t^0} i(nt_s) = i(nt_s), \tag{A.3}$$

as it must also be by definition;

$$\frac{\mathrm{d}^{1/2}}{\mathrm{d}t^{1/2}} i(nt_s) = \frac{1}{t_s^{1/2}} \sum_{j=0}^{n} (-1)^j \frac{\Gamma(3/2)}{\Gamma(j+1)\Gamma(3/2-j)} i([n-j]\,t_s) \tag{A.4}$$

and

$$\frac{\mathrm{d}}{\mathrm{d}t} i(nt_s) = \frac{1}{t_s}\{i(nt_s) - i([n-1]\,t_s)\}. \tag{A.5}$$

Note that equation (A.5) corresponds to the first-order derivative expressed by using the classical first-order finite difference.

A.2. Relationship between $\langle\omega^n\rangle$ and the physiological parameters

The relationship between $\langle\omega^n\rangle$ and the physiological parameters has been previously obtained in Binzoni *et al* (2004) and the derivation follows a rather tedious procedure. Here we report only the intuitive idea and the main result. In practice, the general expression allowing us to obtain equations (6)–(8) has been derived by following the original Bonner and Nossal (1981) method. However, a more general velocity distribution of the red blood cell has been chosen, i.e. by including a supplementary bulk translational velocity, $\vec{V}_{\mathrm{trans}}$, that should better represent the tissue physiology. Coherently, when $\vec{V}_{\mathrm{trans}}$ is set to zero, the original results from Bonner and Nossal results are found. The general expression giving all the possible n-order moments, $\langle\omega^n\rangle$, corresponds to (equations (25) and (26) in Binzoni *et al* (2004))

$$\langle\omega^n\rangle = \frac{2A^2\,\mathrm{dc}^2\beta\,\mathrm{e}^{-2\bar{m}}}{\pi} \sum_{j=1}^{+\infty} \frac{(2\bar{m})^j}{j!} \int_{-\infty}^{+\infty} |\omega|^n \left\{ \int_{-\infty}^{+\infty} \mathrm{e}^{\mathrm{i}\omega\tau} \left[I_1^{\infty}(\tau)\right]^j \mathrm{d}\tau \right\} \mathrm{d}\omega, \tag{A.6}$$

where

$$\left[I_1^{\infty}(\tau)\right]^j = \frac{12^j \xi^j a^{2j}}{\pi} \sum_{N=1}^{+\infty} j^N \frac{(-1)^N \left(\frac{3}{2}\right)^N \left\{\int_0^{\pi} \sin(\theta')^{2N}\,\mathrm{d}\theta'\right\} \tau^{2N}}{\Gamma(N+1)(12\xi a^2 + \langle V_{\mathrm{Brown}}^2 \rangle \tau^2)^{N+j}} \|\vec{V}_{\mathrm{trans}}\|^{2N}. \tag{A.7}$$

Substituting n by 0, 1 or 2, one can directly retrieve equations (6), (7) and (8). The parameters A, dc, β, ξ and a are constants that are not essential in the present context and thus they are simply included in the global constants c_1 and c_2 in equations (6), (7) and (8).

References

Binzoni T, Leung T S, Rüfenacht D and Delpy D T 2006 Absorption and scattering coefficient dependence of laser-Doppler flowmetry models for large tissue volumes *Phys. Med. Biol.* **51** 311–33

Binzoni T, Leung T S, Seghier M L and Delpy D T 2004 Translational and Brownian motion in laser-Doppler flowmetry of large tissue volumes *Phys. Med. Biol.* **49** 5445–58

Binzoni T, Leung T S and Van De Ville D 2009 The photo-electric current in laser-Doppler flowmetry by Monte Carlo simulations *Phys. Med. Biol.* **54** N303–18

Binzoni T and Van De Ville D 2008 Full-field laser-Doppler imaging and its physiological significance for tissue blood perfusion *Phys. Med. Biol.* **53** 6673–94

Bonner R F and Nossal R 1981 Model for laser Doppler measurements of blood flow in tissue *Appl. Opt.* **20** 2097–107

Briers J D 2001 Laser Doppler, speckle and related techniques for blood perfusion mapping and imaging *Physiol. Meas.* **22** R35–66

Briers J D 2007 Laser speckle contrast imaging for measuring blood flow *Opt. Appl.* **37** 139–52
Ciletti M D 2009 *Advanced Digital Design with Verilog HDL* (Upper Saddle River, NJ: Prentice Hall)
Draijer M, Hondebrink E, van Leeuwen T and Steenbergen W 2009a Twente optical perfusion camera: system overview and performance for video rate laser Doppler perfusion imaging *Opt. Express* **17** 3211–25
Draijer M, Hondebrink E, van Leeuwen T and Steenbergen W 2009b Time-domain algorithm for accelerated determination of the first order moment of photo current fluctuations in high speed laser Doppler perfusion imaging *Med. Biol. Eng. Comput.* **47** 1103–9
Ferreira L F, Hueber D M and Barstow T J 2007 Effects of assuming constant optical scattering on measurements of muscle oxygenation by near-infrared spectroscopy during exercise *J. Appl. Physiol.* **102** 358–67
Galucio A C, Deü J-F, Mengué S and Dubois F 2006 An adaptation of the Gear scheme for fractional derivatives *Comput. Methods Appl. Mech. Eng.* **195** 6073–85
Humeau A, Steenbergen W, Nilsson H and Strömberg T 2007 Laser Doppler perfusion monitoring and imaging: novel approaches *Med. Biol. Eng. Comput.* **45** 421–35
Morgan S, Hayes-Gill B and Crowe J 2010 CMOS sensors for imaging blood flow *Opt. Photonics News* **21** 32–7
Podlubny I 1999 *Fractional Differential Equations. An Introduction to Fractional Derivatives, Fractional Differential Equations, Some Methods of Their Solution and Some of Their Applications* (New York: Academic)
Raabe A *et al* 2009 Laser doppler imaging for intraoperative human brain mapping *NeuroImage* **44** 1284–9
Roth C H Jr and John L K 2007 *Digital Systems Design Using VHDL* (Masson, OH: Thomson)
Serov A, Steenbergen W and de Mul F 2002 Laser Doppler perfusion imaging with a complimentary metal oxide semiconductor image sensor *Opt. Lett.* **27** 300–2
Serov A, Steinacher B and Lasser T 2005 Full-field laser Doppler perfusion imaging and monitoring with an intelligent CMOS camera *Opt. Express* **13** 3681–9